

Fast, Simultaneous Optimization of Power Amplifier Input Power and Load Impedance for Power-Added Efficiency and Adjacent-Channel Power Ratio Using the Power Smith Tube

JOSEPH BARKATE, Student Member, IEEE
MATTHEW FLACHSBART, Student Member, IEEE
ZACHARY HAYS, Student Member, IEEE
MATTHEW FELLOWS, Student Member, IEEE
JENNIFER BARLOW, Student Member, IEEE
CHARLES BAYLIS, Member, IEEE

Baylor University
Waco, TX, USA

LAWRENCE COHEN, Senior Member, IEEE
Naval Research Laboratory
Washington, DC, USA

ROBERT J. MARKS, II, Fellow, IEEE
Baylor University
Waco, TX, USA

Reconfigurable adaptive amplifiers are expected to be a critical component of future adaptive and cognitive radar transmitters. This paper details an algorithm to simultaneously optimize input power and load reflection coefficient of a power amplifier device to obtain the largest power-added efficiency (PAE) possible under a predefined constraint on adjacent-channel power ratio (ACPR). The vector-based search relies on estimation of the PAE and ACPR

Manuscript received May 11, 2015; revised September 3, 2015; released for publication October 8, 2015.

DOI. No. 10.1109/TAES.2015.150335.

Refereeing of this contribution was handled by S. Blunt.

This work has been funded under a grant from the National Science Foundation (Award ECCS-1343316).

Authors' addresses: J. Barkate, M. Flachsbart, Z. Hays, M. Fellows, J. Barlow, C. Baylis, R.J. Marks II, Baylor University, Department of Electrical and Computer Engineering, One Bear Place #97356, Waco, TX 76798-7356, USA. L. Cohen, U.S. Naval Research Laboratory, Radar Division, 4555 Overlook Ave., SW, Washington, DC 20375, USA. Corresponding author is C. Baylis, E-mail: (Charles_Baylis@Baylor.edu).

0018-9251/16/\$26.00 © 2016 IEEE

gradients in the three-dimensional power Smith tube. Accurate convergence to the optimum impedance in the Smith chart is demonstrated in simulation and measurement search experiments requiring between 20 and 60 experimental queries. This paper presents a fast search to jointly optimize the input power level and load impedance. This method is feasible for future implementation in real-time reconfigurable power amplifiers.

I. INTRODUCTION

Given increasingly stringent spectral constraints, future radar transmitters will need to be adaptive and reconfigurable to allow operation in different frequency bands and meet various spectral constraints based on nearby wireless activity. Transmitters will have to quickly adjust their transmission spectra, frequency of operation, and circuitry to operate in a dynamically changing spectral environment. Such adjustments will likely need to occur on the order of milliseconds. The power amplifier is a critical component of radar transmitters, and its power efficiency and spectral output are significantly dependent on its loading. We present a new method for simultaneously optimizing the load impedance and the input power to maximize the efficiency, while meeting spectral constraints. This algorithm is designed to be used in real-time optimization for reconfiguring the load impedance and input power of an adaptive radar transmitter amplifier, and so a significant goal of the algorithm's design is to minimize the number of experimental queries. The optimization is based on two well-known metrics. Efficiency is measured by the power-added efficiency (PAE), which is the added radio frequency power divided by the direct current supply power. Spectral spreading is measured by the adjacent-channel power ratio (ACPR), which is the ratio of the power in a defined adjacent channel to the power in the designated operating channel.

Adaptive radar has been a topic of discussion since the early 1970s [1]. In the modern era of tight spectrum allocations, adaptive radar will need reconfigurable circuitry to allow real-time adjustments to change spectral output, operating frequency, and power efficiency. Lu et al. and Vaka-Heikkila and Rebeiz describe use of microelectromechanical system switches to build amplifiers with adaptive output matching networks [2, 3]. Deve et al. present an adaptive impedance tuner capable of adjusting operating frequency between 1 and 3 GHz, a frequency range useful for many sensing applications [4]. Sun et al. predict the criticality of intelligent impedance matching with minimized tuning iterations for reconfigurable transmitters [5]. Real-time antenna impedance matching has been demonstrated by Sun and Sun and Lau [6, 7], and Qiao et al. demonstrate the use of a genetic algorithm to tune an amplifier in real time [8], although du Plessis and Abrie predict that genetic algorithms will be slow in tuning for many applications [9]. Much of the previous work in impedance tuning has been performed for communications applications, but Baylis et al. describe the importance of reconfigurable

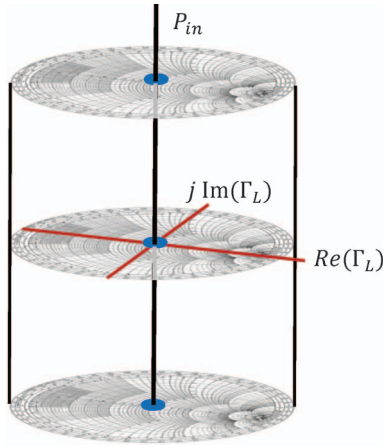


Fig. 1. The power Smith tube. The vertical axis represents the input power, while the horizontal cross section of the tube is a conventional Smith chart [18].

power amplifiers in solving the radar-communications coexistence problem [10]. Recent radar developments include design of adaptive waveforms and circuits that can optimize for power efficiency and spectral compliance, including the effects of transmitter distortion. Blunt et al. describe the use of polyphase-coded frequency modulation waveforms for good power efficiency and spectral performance [11] and present optimization of these waveforms with transmitter amplifier distortion considered, both via a model and in actual measurements [12].

The variation of PAE and ACPR with both load reflection coefficient Γ_L and input power P_{in} is well documented. Snider describes how the load impedance providing optimal efficiency varies with input power level and demonstrates that the output power is significantly dependent on both the load impedance and the input power level [13], and Nemati et al. show variation of the optimum PAE load impedance with changing input power [14]. Fu and Mortazawi show the design of a reconfigurable power amplifier using tunable varactors and also show that the load impedance in the Smith chart providing optimum efficiency is different for different output power levels [15]. Hajji et al. show that a change in input power can be useful in obtaining constant intermodulation rejection [16], related to the adjacent-channel spreading of amplifiers under broadband signal excitation. Load modulation to provide efficiency in Doherty amplifiers is discussed by Nam et al. [17].

Our previous work introduces the input power Smith tube (Fig. 1) to visualize how a criterion (such as PAE or ACPR) varies with both load reflection coefficient and input power [18]. Previous Smith chart extensions include a spherical extension of the Smith chart to consider both positive and negative resistances in circuit design [19, 20], a Smith chart generalization allowing fractional circuit elements to be considered [21], and an adjusted Smith chart for design with lossy transmission lines [22].

The purpose of the present paper is to show how an optimum combination of Γ_L and P_{in} can be obtained quickly, using a small number of measurements, through a fast search algorithm in the power Smith tube. The desired optimization is an example of biobjective optimization [23, 24] and is applied to the well-known trade-off of linearity and efficiency [25, 26]. A previous paper by our group demonstrates optimization for linearity and efficiency using only the real and imaginary parts of Γ_L as the input parameters [27], and the present paper extends the solution of this problem to a third dimension, allowing simultaneous optimization of input power with Γ_L to provide the highest PAE possible under ACPR constraints.

Section II presents the basics of the search algorithm to be applied in the Smith tube. Section III describes simulation results of the algorithm's application. Section IV provides results from measurement testing of the algorithm. Finally, Section V provides conclusions based on the presented results.

II. ALGORITHM DETAILS

The search algorithm is based on estimation of the PAE and ACPR gradients within the three-dimensional input power Smith tube. First, the input power, on the vertical axis of the Smith tube, is normalized so that the user-defined maximum input power is assigned the value 1 and the user-defined minimum input power is assigned the value -1 . This scales the vertical limitations of the cylindrical search space (the Smith tube) to the same dimensions as the planar values of Γ_L in the horizontal dimension. The normalized input power p_{in} (with a lowercase "p") is defined as follows (all power values are in dBm, decibels with respect to 1 milliwatt, for this paper).

$$p_{in} = 2 \frac{P_{in} - P_{in,min}}{P_{in,max} - P_{in,min}} - 1 \quad (1)$$

This equation normalizes the range of P_{in} to set the minimum to -1 and the maximum to 1. The normalized input power p_{in} represents the input power for purposes of calculating and evaluating gradients.

Although the three-dimensional search is limited by the power Smith tube's cylindrical space, the search vectors can be laid out in Cartesian dimensions, because the horizontal coordinates represent the real and imaginary parts of Γ_L . The vertical coordinate p_{in} provides the third of the three Cartesian dimensions. Using Cartesian coordinates allows direct extension of the search space used in the two-dimensional algorithm for the same objectives [27].

A search vector \bar{v} can be added to a candidate in the Smith tube to find the subsequent candidate in the search. When the candidate from which the search is operating does not possess an acceptable ACPR value, this search vector is defined as follows:

$$\bar{v} = \hat{a}D_a + \hat{b}D_b, \quad (2)$$

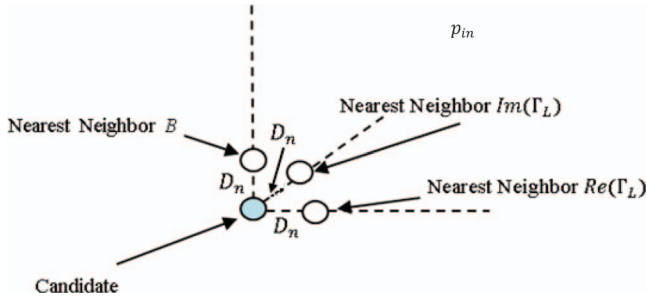


Fig. 2. Gradient evaluation in three dimensions.

where

$$D_a = \frac{D_s |ACPR_{meas} - ACPR_{target}|}{2 |ACPR_{worst} - ACPR_{target}|} \quad (3)$$

and

$$D_b = \frac{D_s |\theta_{meas} - \theta_{target}|}{2 \theta_{target}}. \quad (4)$$

D_s is the search distance parameter and is provided by the user. It provides scaling for both components of the search vector [(3) and (4)]. $ACPR_{meas}$ is the measured value of ACPR at the present candidate point. $ACPR_{target}$ is the maximum acceptable value of ACPR. $ACPR_{worst}$ is the largest value of ACPR measured to this point in the search. θ is the angle between vectors \hat{a} and \hat{b} . In (2), the vectors \hat{a} and \hat{b} represent vectors in the direction of ACPR steepest descent and the bisector between the ACPR steepest descent and PAE steepest ascent vectors. On the Pareto optimum locus, which is the curve of constrained solutions, the gradients will be oppositely directed [6], and the value of θ (the half-angle between the gradients) will be 90° . Thus, $\theta_{target} = 90^\circ$ in (4). θ_{meas} is the measured value of θ at the candidate under consideration. Fig. 2 shows that the gradients can be evaluated in the three-dimensional space. If PAE is represented by the variable p , the gradient for the PAE is given in terms of the unit coordinate vectors $\hat{\Gamma}_r$, $\hat{\Gamma}_i$, and \hat{p}_{in} by

$$\nabla p = \hat{\Gamma}_r \frac{\partial p}{\partial \Gamma_r} + \hat{\Gamma}_i \frac{\partial p}{\partial \Gamma_i} + \hat{p}_{in} \frac{\partial p}{\partial p_{in}}. \quad (5)$$

The partial derivatives to calculate this gradient are estimated from a measurement separated from the candidate in the Smith tube by a neighboring-point distance D_n in each coordinate direction, as shown in Fig. 2. From a measurement of the change in power Δp at a change in the real part of the load reflection coefficient, Γ_r , the partial-derivative estimation follows as

$$\frac{\partial p}{\partial \Gamma_r} \approx \frac{\Delta p}{\Delta \Gamma_r} = \frac{\Delta p}{D_n}. \quad (6)$$

From a measurement of the change in power for a change in the imaginary part of the load reflection coefficient, Γ_i , the partial-derivative estimation follows as

$$\frac{\partial p}{\partial \Gamma_i} \approx \frac{\Delta p}{\Delta \Gamma_i} = \frac{\Delta p}{D_n}. \quad (7)$$

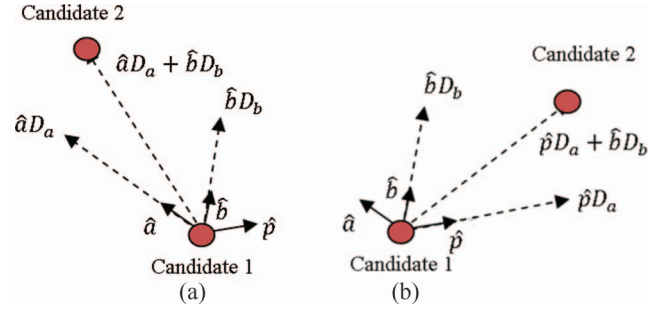


Fig. 3. Search vectors in three dimensions in the cases in which (a) ACPR is not within constraints and (b) ACPR is within constraints.

Finally, from a measurement of the change in power Δp at a change in p_{in} , the calculation follows as

$$\frac{\partial p}{\partial p_{in}} \approx \frac{\Delta p}{\Delta p_{in}} = \frac{\Delta p}{D_n}. \quad (8)$$

Because normalized power p_{in} (lowercase) is being used, as defined by (1), the same step D_n is used in the vertical direction for the partial derivative estimation as for the horizontal directions. This completes the estimation of the gradient vector given by (5). The unit vector in the direction of increasing PAE can be taken by dividing the gradient by its magnitude:

$$\hat{p} = \frac{\nabla p}{|\nabla p|} \quad (9)$$

An approach similar to (5) through (8) can be used to estimate the gradient for ACPR. Because minimization is desired for the ACPR, the direction of optimal travel is given by a unit vector \hat{a} oriented oppositely to the ACPR gradient:

$$\hat{a} = -\frac{\nabla a}{|\nabla a|}. \quad (10)$$

The three-dimensional bisector of \hat{a} and \hat{p} is defined as the arithmetic mean of the vectors \hat{p} and \hat{a} . Because \hat{a} and \hat{p} are both unit vectors, the mean (bisector) given by

$$\hat{b} = \frac{1}{2} (\hat{a} + \hat{p}) \quad (11)$$

is also a unit vector.

Fig. 3 shows the resultant search vectors for the cases when ACPR at the present candidate is out of compliance (Fig. 3a) and when ACPR at the present candidate is within compliance (Fig. 3b). When the ACPR is in compliance, the search vector (2) is changed to have a component in the \hat{p} direction instead of the \hat{a} direction:

$$\bar{v} = \hat{p} D_a + \hat{b} D_b. \quad (12)$$

A noticeable result of using (2) when the search is out of ACPR compliance and (12) when the search is in compliance is that the search firsts attempts to try to reach the region of ACPR compliance. When the initiating candidate is out of compliance, (2) is used, meaning that the search vector has a component of \hat{a} , which causes a

component of travel toward the ACPR minimum. An \hat{a} component will be present in each search vector until the region of ACPR compliance is reached. When an initiating candidate is inside the region of ACPR compliance, (12) is used, meaning that the \hat{a} component of (2) is replaced by a \hat{p} component of the same magnitude. This means that the search replaces its initial quest for the acceptable region by going toward the PAE optimum. It progresses with this component directed toward the optimum PAE point, as long as it remains in compliance. In the results shown in the following section, note that the first effort of each search is to reach the region of ACPR compliance. If the starting point of the search is outside the ACPR compliance region, this can result in an initial downward trajectory of the search for several candidates, followed by a subsequent upward trajectory once the search enters the ACPR compliance region.

The speed and resolution of the algorithm's convergence are dependent on the starting point and the parameter values selected for the search distance D_s and neighboring-point distance D_n . Although further analysis could be performed to find the optimal values of these parameters given domain expertise and desired outcomes, this topic is saved for a later paper. In general, larger values of D_s are suggested for use if the vicinity of the end point is unknown; if the search is believed to start near the optimum, then a smaller value of D_s may reduce the number of measurements.

If the search reaches the region of ACPR compliance and then tries to leave, the search distance parameter D_s is divided by two, and the search returns to the last candidate in the acceptable ACPR region and calculates a new search vector using the modified D_s . In addition to this penalization for leaving the acceptable region, the search vector tends to get smaller as it approaches the optimum, because $ACPR_{meas}$ tends to approach $ACPR_{target}$ and θ_{meas} tends to approach θ_{target} , decreasing the search vector components according to (3) and (4), respectively. When the size of the search vector $|\vec{v}|$ decreases below a prespecified value (often the same as D_n), the search ends, and the measured point with the highest PAE that meets ACPR requirements is declared the constrained optimum.

III. SIMULATION RESULTS

The algorithm was first tested in simulations using a nonlinear transistor model in the Advanced Design System (ADS) simulator from Keysight Technologies. A cosimulation was constructed using MATLAB to perform algorithm-controlled ADS simulations. In the cosimulation, MATLAB is used to control an ADS nonlinear circuit simulation when supplied a netlist by ADS, including the values of P_{in} and Γ_L , and then MATLAB reads the results from ADS and performs algorithmic decisions, recalling ADS for each required circuit simulation in the algorithm's execution. For the design, a constraint of $ACPR \leq -40$ dBc was imposed on the design. The goal was to obtain the highest PAE, while

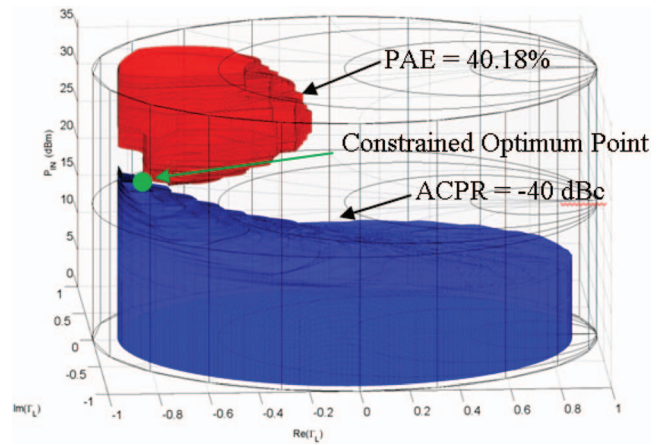


Fig. 4. Constant ACPR surface from simulation data for $ACPR = -40$ dBc and PAE surface representing the maximum PAE from simulated load-pull data. The ACPR-constrained optimum solution occurs where the two surfaces intersect; the surfaces are collinear at this point. The ACPR-constrained optimum occurs at location $\Gamma_L = 0.80/180^\circ$ at a power level of 21.75 dBm, where PAE = 40.18% and ACPR = -40.23 dBc.

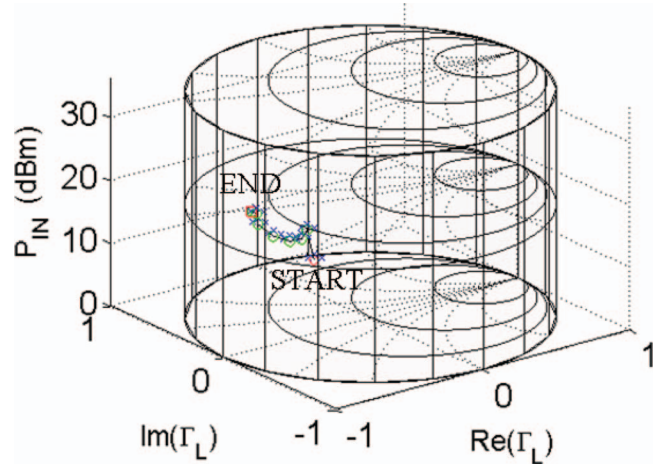


Fig. 5. Simulated search algorithm trajectory through the power Smith tube using $D_s = 1$, input power range $0 \text{ dBm} \leq P_{in} \leq 36 \text{ dBm}$, and starting location $\Gamma_L = 0.50/90^\circ$, $P_{in} = 5 \text{ dBm}$. The search required 29 measured points and converged to the end point $\Gamma_L = 0.79/-178.6^\circ$ and $P_{in} = 21.58 \text{ dBm}$, where PAE = 41.13% and ACPR = -40.08 dBc.

meeting this ACPR constraint. For comparison with the algorithm results, load-pull simulations spanning the Smith chart were performed at multiple input power levels and are shown in Fig. 4, as presented in [6]. This exhaustive measurement shows that the ACPR-constrained optimum point is at $P_{in} = 21.75 \text{ dBm}$ and $\Gamma_L = 0.80/180^\circ$. The maximum PAE providing $ACPR \leq -40$ dBc is 40.18% at this point.

Simulation tests of the algorithm were performed using a stepsize $D_s = 1.5$, neighboring-point distance $D_n = 0.05$, and input power range $0 \text{ dBm} \leq P_{in} \leq 36 \text{ dBm}$. Because D_n and D_s have units consistent with the dimensions of the Smith chart, they possess the same units as load reflection coefficient Γ_L and are unitless. Figure 5 shows the trajectory of a search

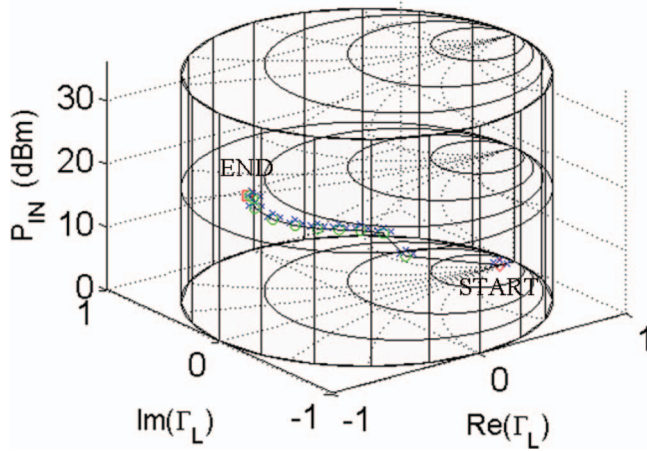


Fig. 6. Simulated search algorithm trajectory through the power Smith tube using $D_s = 1$, input power range $0 \text{ dBm} \leq P_{in} \leq 36 \text{ dBm}$, and starting location $\Gamma_L = 0.90/0^\circ$, $P_{in} = 0 \text{ dBm}$. The search required 42 measured points and converged to the end point $\Gamma_L = 0.77/176.4^\circ$ and $P_{in} = 21.21 \text{ dBm}$, where PAE = 41.44% and ACPR = -40.05 dBc .

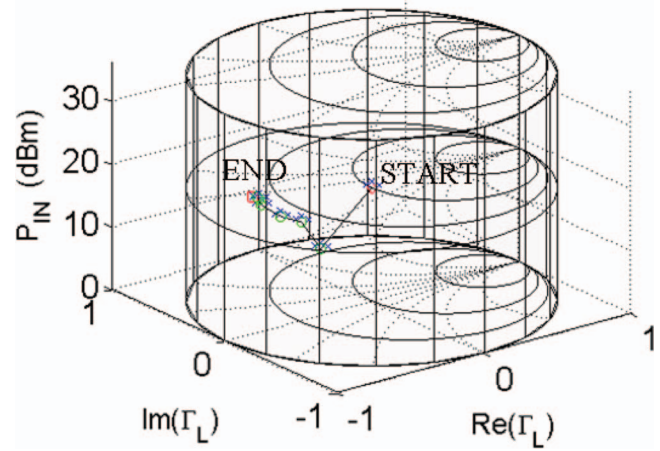


Fig. 8. Simulated search algorithm trajectory through the power Smith tube using $D_s = 1$, input power range $0 \text{ dBm} \leq P_{in} \leq 36 \text{ dBm}$, and starting location $\Gamma_L = 0.00/0^\circ$, $P_{in} = 18 \text{ dBm}$. The search required 28 measured points and converged to the end point $\Gamma_L = 0.76/175.7^\circ$ and $P_{in} = 20.89 \text{ dBm}$, where PAE = 40.77% and ACPR = -40.14 dBc .

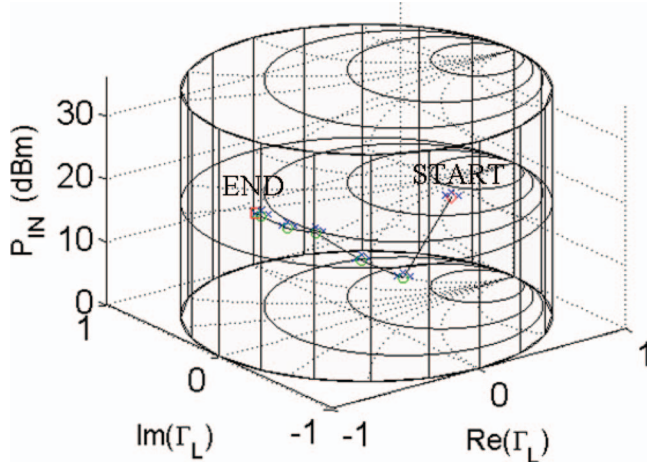


Fig. 7. Simulated search algorithm trajectory through the power Smith tube using $D_s = 1.50$, input power range $0 \text{ dBm} \leq P_{in} \leq 36 \text{ dBm}$, and starting location $\Gamma_L = 0.75/-90^\circ$, $P_{in} = 25 \text{ dBm}$. The search required 26 measured points and converged to the end point $\Gamma_L = 0.75/-179.6^\circ$ and $P_{in} = 21.07 \text{ dBm}$, where PAE = 40.76% and ACPR = -40.76 dBc .

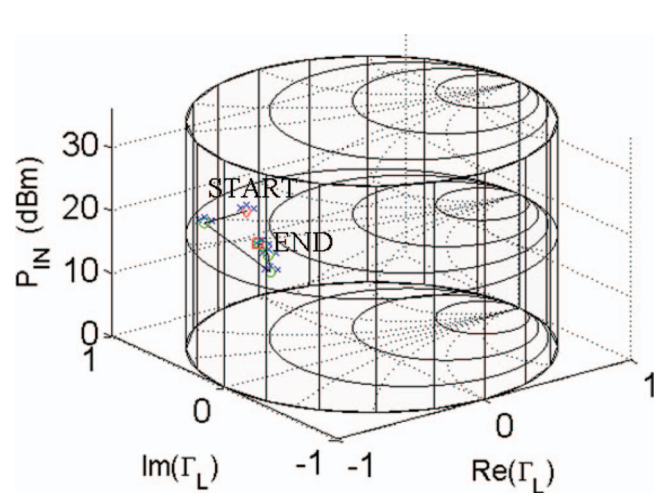


Fig. 9. Simulated search algorithm trajectory through the power Smith tube using $D_s = 1$, input power range $0 \text{ dBm} \leq P_{in} \leq 36 \text{ dBm}$, and starting location $\Gamma_L = 0.85/180^\circ$, $P_{in} = 27 \text{ dBm}$. The search required 25 measured points and converged to the end point $\Gamma_L = 0.76/179.3^\circ$ and $P_{in} = 21.23 \text{ dBm}$, where PAE = 40.89% and ACPR = -40.18 dBc .

starting from $\Gamma_L = 0.5/90^\circ$, $P_{in} = 5 \text{ dBm}$. A total of 33 measured points was required for the search to converge to the end parameter values of $\Gamma_L = 0.79/-178.6^\circ$ and $P_{in} = 21.58 \text{ dBm}$. At this end point, PAE = 41.13% and ACPR = -40.08 dBc were obtained. Fig. 6 shows the search trajectory for a starting point of $\Gamma_L = 0.80/0^\circ$, $P_{in} = 0 \text{ dBm}$. Notice that while the starting conditions were very different in both cases, the end point values of Γ_L , P_{in} , PAE, and ACPR are very similar. This indicates that both searches converge to approximately the same location in the Smith tube.

Figs. 7 through 9 show the search results for additional different starting combinations of Γ_L and P_{in} . Table I summarizes the search results for the different starting combinations. The results show that the final values of PAE vary less than 1%. The ending ACPR values are all

within 0.2 dB of the -40-dBc limiting value. The end point Γ_L coordinates are also similar, and the variation across end point P_{in} values is less than 1 dB. The results all compare well with the optimum value obtained from the exhaustive load-pull search. Interestingly, the PAE values obtained from the algorithm are all slightly better than the optimum obtained through the exhaustive measurement, because the points measured in the Smith tube for the exhaustive measurement are spaced in a way that the resolution of the optimum's determination is less than the shorter, algorithm-based search. This shows that excellent resolution can be obtained by the fast search, even if no initial information is known about the location of the optimum.

TABLE I
Simulation Results for Different Starting Reflection Coefficients

Start Γ_L	Start P_{in} (dBm)	End Γ_L	End P_{in} (dBm)	End ACPR (dBc)	End PAE (%)	Number of Measurements
0.5/90°	5	0.79/-178°	21.59	-40.08	41.13	29
0.9/0°	0	0.77/176°	21.21	-40.05	41.44	42
0.75/-90°	25	0.75/-180°	21.07	-40.15	40.76	26
0	18	0.76/176°	20.89	-40.14	40.78	28
0.85/180°	27	0.76/179°	21.23	-40.18	40.88	25

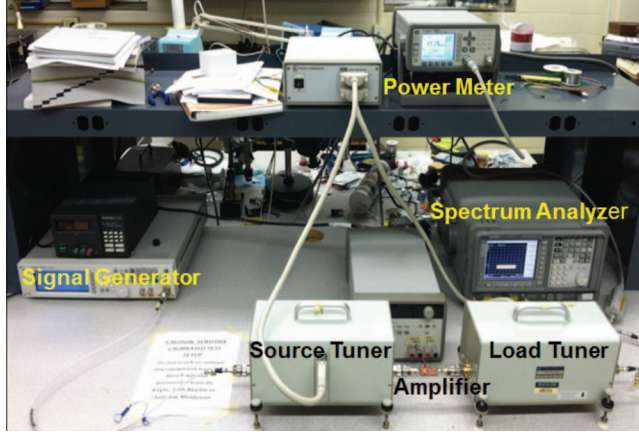


Fig. 10. Measurement setup.

IV. MEASUREMENT RESULTS

The algorithm was measurement tested using the nonlinear load-pull test bench in the laboratory of the authors (Fig. 10). The input waveform is supplied by the signal generator with variable input power. Measurements of PAE are performed with the power meter, and a spectrum analyzer is used to measure ACPR. The algorithm was tested on a Skyworks SKY5017-70LF InGaP packaged amplifier. This device is different from the modeled device used for the simulation test of the algorithm, providing unrelated behavior for examining algorithm performance. Measurement tests of the algorithm were performed using a stepsize $D_s = 1.5$, neighboring-point distance $D_n = 0.05$, and input power range $-5 \text{ dBm} \leq P_{in} \leq 2 \text{ dBm}$. An ACPR limit of -27.5 dBc was specified for this search.

For comparison with the algorithm results, Fig. 11 shows a plot of the constant ACPR surface for the -27.5-dBc limiting value, extracted from exhaustive, traditional load-pull measurements performed at multiple P_{in} values. The maximum PAE value, as assessed by the traditional load pull, is 7.39%, obtained for $\Gamma_L = 0.47/-41.5^\circ$ and $P_{in} = 1.5 \text{ dBm}$.

Figs. 12 through 16 show the search trajectory for different starting combinations of Γ_L and P_{in} . The results of the searches show excellent correspondence to each other, as summarized in Table II. Variation in end point P_{in} across the five searches is less than 0.5 dB. All ACPR end point values are beneath the limit and within 0.4 dB of the limiting value. End point PAE varies by less than 0.5%

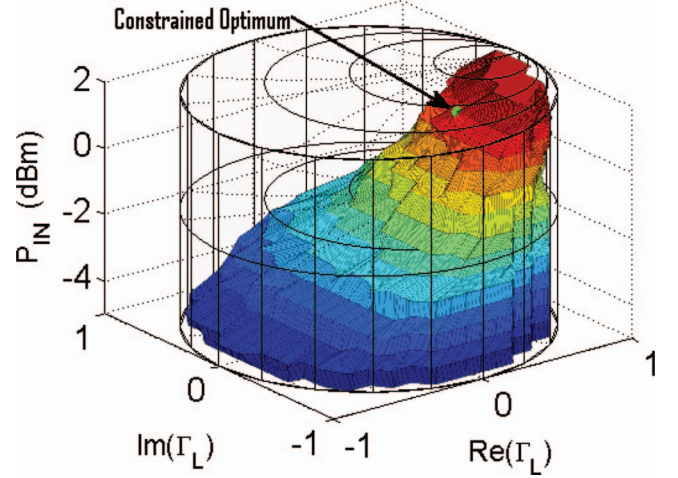


Fig. 11. Constant ACPR surface from measurement data for ACPR = -27.5 dBc , with the constrained optimum point indicated.

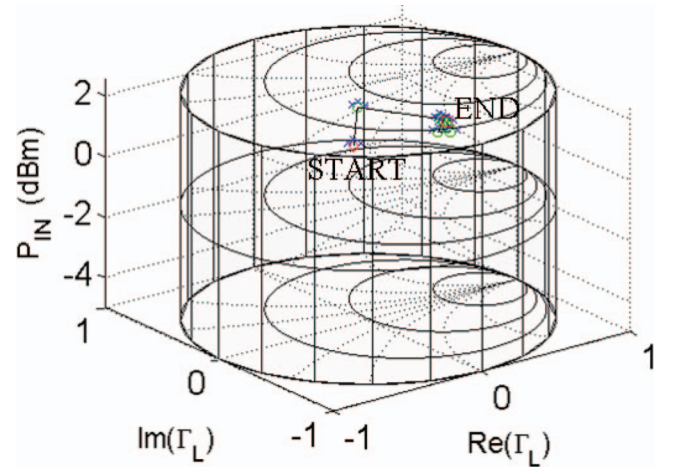


Fig. 12. Measured search algorithm trajectory through the power Smith tube using $D_s = 1$, $D_n = 0.05$, input power range $-5 \text{ dBm} \leq P_{in} \leq 2 \text{ dBm}$, and starting location $\Gamma_L = 0.6/-135^\circ$, $P_{in} = 2 \text{ dBm}$. The search required 31 measured points and converged to the end point $\Gamma_L = 0.42/-44.32^\circ$ and $P_{in} = 1.60 \text{ dBm}$, where PAE = 7.32% and ACPR = -27.55 dBc .

across all of the searches. The number of measurements ranges from 23 to 39. As in the simulation case, the number of measurements required appears to be dependent on factors, including the search starting point location relative to the optimum point.

TABLE II
Measurement Results for Different Starting Reflection Coefficients

Start Γ_L	Start P_{in} (dBm)	End Γ_L	End P_{in} (dBm)	End ACPR (dBm)	End PAE (%)	Number of Measurements
$0.6/-135^\circ$	2.0	$0.42/-44^\circ$	1.60	-27.55	7.32	31
0	0.0	$0.45/-47^\circ$	1.58	-27.86	7.05	23
$0.8/0^\circ$	-3.0	$0.43/-24^\circ$	1.57	-27.51	7.49	35
$0.9/180^\circ$	-4.0	$0.42/-40^\circ$	1.67	-27.80	7.23	39
$0.75/45^\circ$	1.5	$0.39/-38^\circ$	1.21	-27.51	7.29	24

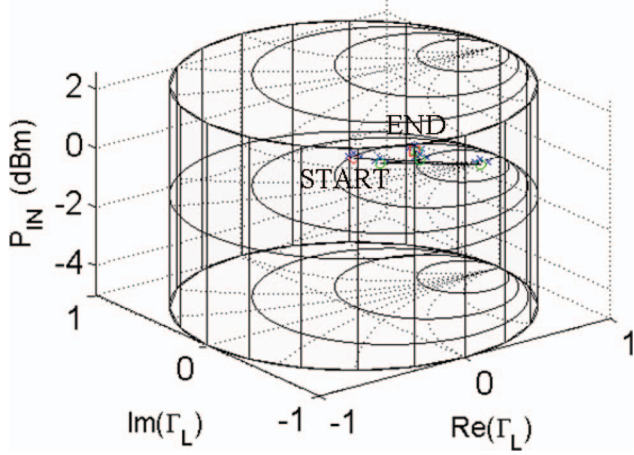


Fig. 13. Measured search algorithm trajectory through the power Smith tube using $D_s = 1$, $D_n = 0.05$, input power range $-5 \text{ dBm} \leq P_{in} \leq 2 \text{ dBm}$, and starting location $\Gamma_L = 0$, $P_{in} = 0 \text{ dBm}$. The search required 19 measured points and converged to the end point $\Gamma_L = 0.45/-46.61^\circ$ and $P_{in} = 1.58 \text{ dBm}$, where PAE = 7.05% and ACPR = -27.86 dBc.

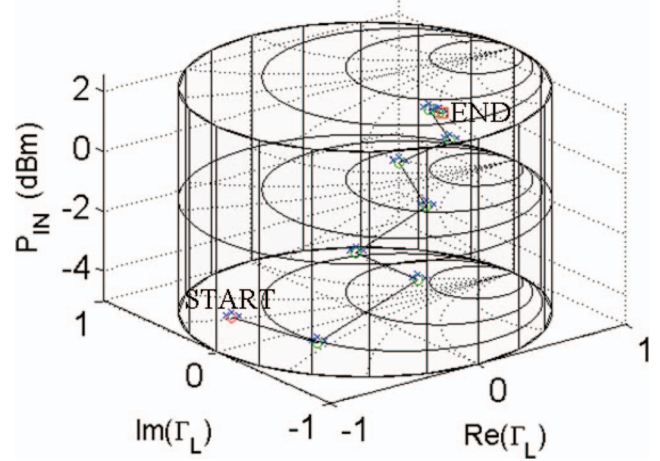


Fig. 15. Measured search algorithm trajectory through the power Smith tube using $D_s = 1$, $D_n = 0.05$, input power range $-5 \text{ dBm} \leq P_{in} \leq 2 \text{ dBm}$, and starting location $\Gamma_L = 0.9/180^\circ$, $P_{in} = -4 \text{ dBm}$. The search required 39 measured points and converged to the end point $\Gamma_L = 0.42/-40.33^\circ$ and $P_{in} = 1.67 \text{ dBm}$, where PAE = 7.23% and ACPR = -27.80 dBc.

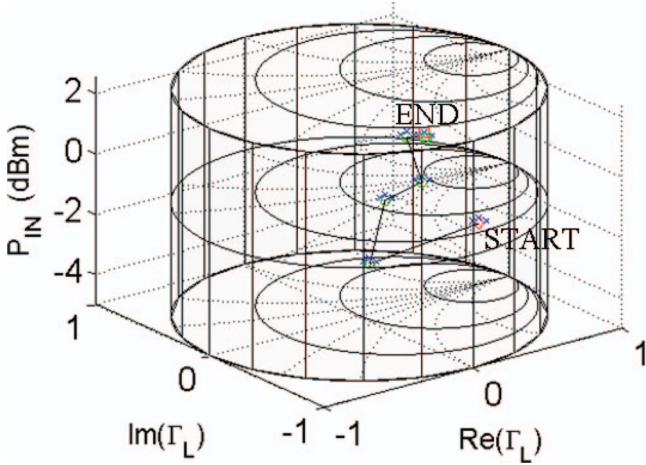


Fig. 14. Measured search algorithm trajectory through the power Smith tube using $D_s = 1$, $D_n = 0.05$, input power range $-5 \text{ dBm} \leq P_{in} \leq 2 \text{ dBm}$, and starting location $\Gamma_L = 0.8/0^\circ$, $P_{in} = -3 \text{ dBm}$. The search required 35 measured points and converged to the end point $\Gamma_L = 0.43/-24.12^\circ$ and $P_{in} = 1.57 \text{ dBm}$, where PAE = 7.49% and ACPR = -27.51 dBc.

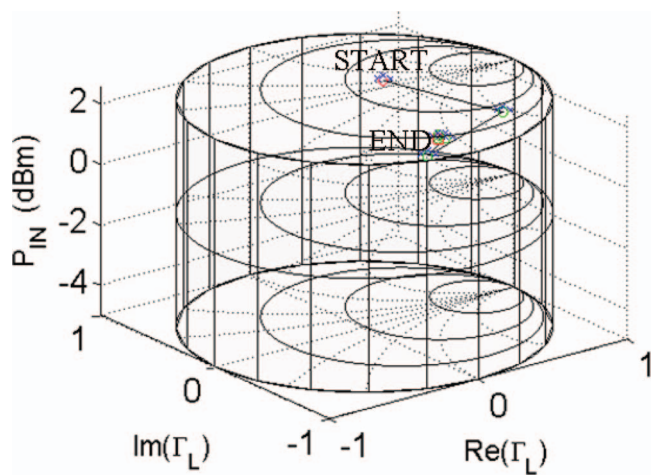


Fig. 16. Measured search algorithm trajectory through the power Smith tube using $D_s = 1$, $D_n = 0.05$, input power range $-5 \text{ dBm} \leq P_{in} \leq 2 \text{ dBm}$, and starting location $\Gamma_L = 0.75/45^\circ$, $P_{in} = 1.5 \text{ dBm}$. The search required 24 measured points and converged to the end point $\Gamma_L = 0.39/-38.37^\circ$ and $P_{in} = 1.21 \text{ dBm}$, where PAE = 7.29% and ACPR = -27.51 dBc.

V. CONCLUSIONS

A fast search algorithm has been presented and validated for simultaneous optimization of power amplifier load reflection coefficient and input power for maximum

PAE, while meeting ACPR requirements. The search has been demonstrated with simulations and measurements using the search space of the power Smith tube. In both simulation and measurement, the results of searches taken from multiple starting points show excellent convergence

as compared with traditional load-pull evaluations performed at multiple values of input power. Furthermore, the results show the ability to improve the resolution of the solution. This results in the ability to obtain improved PAE, while meeting ACPR requirements without having to perform load-pull measurements over very closely spaced input power values. Excellent repeatability of the algorithm from multiple starting points is observed in both the simulation and measurement results.

ACKNOWLEDGMENT

The authors thank Keysight Technologies for cost-free loan of the Advanced Design System simulation software.

REFERENCES

- [1] Brennan, L. E., and Reed, I. S. Theory of adaptive radar. *IEEE Transactions on Aerospace and Electronic Systems*, **AES-9**, 2 (Mar. 1973), 237–252.
- [2] Lu, Y., Peroulis, D., Mohammadi, S., and Katehi, L. A MEMS reconfigurable matching network. *IEEE Microwave and Wireless Components Letters*, **13**, 10 (Oct. 2003), 437–439.
- [3] Vaka-Heikkila, T., and Rebeiz, G. A 4–18 GHz reconfigurable RF MEMS matching network for power amplifier applications. *International Journal of RF and Microwave Computer-Aided Engineering*, **14**, 4 (July 2004), 356–372.
- [4] Deve, N., Kouki, A., and Nerguizian, V. A compact size reconfigurable 1–3 GHz impedance tuner suitable for RF MEMS applications. In *Proceedings of the 16th International Conference on Microelectronics*, Tunis, Tunisia, Dec. 2004, 101–104.
- [5] Sun, Y., Moritz, J., and Zhu, X. Adaptive impedance matching and antenna tuning for green software-defined and cognitive radio. In *Proceedings of the 54th IEEE International Midwest Symposium on Circuits and Systems*, Seoul, Korea, 2011, 1–4.
- [6] Sun, Y. Evolutionary tuning method for automatic impedance matching in communication systems. In *Proceedings of the 1998 IEEE International Conference on Electronics, Circuits and Systems*, Lisboa, Portugal, 1998, 73–77.
- [7] Sun, Y., and Lau, W. K. Antenna impedance matching using genetic algorithms. In *Proceedings of the IEE Conference on Antennas and Propagation*, York, United Kingdom, Aug. 1999, 31–36.
- [8] Qiao, D., Molino, R., Lardizabal, S., Pillans, B., Asbeck, P., and Jerinic, G. An intelligently controlled RF power amplifier with a reconfigurable MEMS-varactor tuner. *IEEE Transactions on Microwave Theory and Techniques*, **53**, 3, (Mar. 2005), 1089–1095.
- [9] du Plessis, W., and Abrie, P. Lumped impedance matching using a hybrid genetic algorithm. *Microwave and Optical Technology Letters*, **37**, 3 (May 2003), 210–212.
- [10] Baylis, C., Fellows, M., Cohen, L., and Marks, R. J., II. Solving the spectrum crisis: intelligent, reconfigurable microwave transmitter amplifiers for cognitive radar. *IEEE Microwave Magazine*, **15**, 5 (July 2014), 94–107.
- [11] Blunt, S. D., Cook, M., Jakabosky, J., de Graaf, J., and Perrins, E. Polyphase-coded FM (PCFM) radar waveforms, part I: implementation. *IEEE Transactions on Aerospace and Electronic Systems*, **50**, 3 (July 2014), 2218–2229.
- [12] Blunt, S. D., Jakabosky, J., Cook, M., Stiles, J., Seguin, S., and Mokole, E. L. Polyphase-coded (PCFM) radar waveforms, part II: optimization. *IEEE Transactions on Aerospace and Electronic Systems*, **50**, 3 (July 2014), 2230–2241.
- [13] Snider, D. M. A Theoretical analysis and experimental confirmation of the optimally loaded and overdriven RF power amplifier. *IEEE Transactions on Electron Devices*, **ED-14**, 12 (Dec. 1967), 851–857.
- [14] Nemati, H. M., Fager, C., Gustavson, U., Jos, R., and Zirath, H. Design of varactor-based tunable matching networks for dynamic load modulation of high power amplifiers. *IEEE Transactions on Microwave Theory and Techniques*, **57**, 5 (May 2009), 1110–1118.
- [15] Fu, J.-S., and Mortazawi, A. Improving power amplifier efficiency and linearity using a dynamically controlled tunable matching network. *IEEE Transactions on Microwave Theory and Techniques*, **56**, 12 (Dec. 2008), 3239–3244.
- [16] Hajji, R., Beaugerard, F., and Ghannouchi, F. M. Multitone power and intermodulation load-pull characterization of microwave transistors suitable for linear SSPA's design. *IEEE Transactions on Microwave Theory and Techniques*, **45**, 7 (July 1997), 1093–1099.
- [17] Nam, J., Shin, J.-H., and Kim, B. A handset power amplifier with high efficiency at a low level using load-modulation technique. *IEEE Transactions on Microwave Theory and Techniques*, **53**, 8 (Aug. 2005), 2639–2644.
- [18] Barkate, J., Fellows, M., Barlow, J., Baylis, C., and Marks, R. J., II. The Power Smith Tube: joint optimization of power amplifier input power and load impedance for power-added efficiency and adjacent-channel power ratio. In *Proceedings of the IEEE Wireless and Microwave Technology Conference*, Cocoa Beach, FL, Apr. 2015.
- [19] Zelle, C. A spherical representation of the Smith chart. *IEEE Microwave Magazine*, **8**, 3, (June 2007), 60–66.
- [20] Wu, Y., Zhang, Y., Liu, Y., and Huang, H. Theory of the spherical generalized Smith chart. *Microwave and Optical Technology Letters*, **51**, 1 (Nov. 2008), 95–97.
- [21] Shamin, A., Radwan, A. G., and Salama, K. N. Fractional Smith chart theory. *IEEE Microwave and Wireless Components Letters*, **21**, 3 (Mar. 2011), 117–119.
- [22] Kretzschmar, J., and Schoonaert, D. Smith charts for lossy transmission lines. *Proceedings of the IEEE*, **57**, 9 (Sep. 1969), 1658–1660.
- [23] Martin, J., Baylis, C., Cohen, L., de Graaf, J., and Marks, R. J., II. A peak-search algorithm for load-pull optimization of power-added efficiency and adjacent-channel power ratio. *IEEE Transactions on Microwave Theory and Techniques*, **62**, 8 (Aug. 2014), 1772–1783.
- [24] Miettinen, K. *Nonlinear Multiobjective Optimization*. Boston: Kluwer Academic Publishers, 1998.
- [25] Baylis, C., Wang, L., Moldovan, M., Martin, J., Miller, H., Cohen, L., and de Graaf, J.

Designing transmitters for spectral conformity: power amplifier design issues and strategies.

- [26] Ubostad, M., and Olavsbraten, M.
Linearity performance of an RF power amplifier under different bias and load conditions with and without DPD.

In *Proceedings of the 2010 IEEE Radio and Wireless Symposium Digest*, New Orleans, LA, 2010, 232–235.

- [27] Fellows, M., Baylis, C., Martin, J., Cohen, L., and Marks, R. J., II.
Direct algorithm for the Pareto load-pull optimization of power-added efficiency and adjacent-channel power ratio. *IET Radar, Sonar & Navigation*, **8**, 9 (Dec. 2014), 1280–1287.

Joseph Barkate received the B.S. degree in electrical and computer engineering from Baylor University in 2014. He is currently working toward the M.S. degree in electrical and computer engineering and is focusing his research on intelligently optimizable power amplifiers.

Matthew Flachsbart received the B.S. degree in electrical and computer engineering from Baylor University in 2015. His research has focused on the development and implementation of algorithms for circuit optimizations, in addition to the design of power amplifiers with reconfigurable matching networks.

Zachary Hays is a student at Baylor University, where he plans to complete the B.S. degree in electrical and computer engineering in 2016. His research focuses on the development of algorithms for simultaneous optimization of multiple parameters in radar power amplifiers.

Matthew Fellows (S'15) completed the B.S. and M.S. degrees in electrical and computer engineering at Baylor University in 2012 and 2014, respectively. He is currently pursuing his Ph.D. degree at Baylor. His research is focusing on the creation of algorithms for the joint optimization of radar transmitter power amplifier circuitry and waveforms. He has published several papers related to his areas of interest.

Jennifer Barlow received the B.S. degree in electrical and computer engineering from Baylor University in 2015. Her research has focused on intelligent load-pull measurements for optimizable power amplifiers, as well as the design of power amplifiers with reconfigurable matching networks.



Charles Baylis (S'03—M'08) is an associate professor in the Department of Electrical and Computer Engineering at Baylor University, where he directs the Wireless and Microwave Circuits and Systems (WMCS) Program. Dr. Baylis received the B.S., M.S., and Ph.D. degrees in electrical engineering from the University of South Florida in 2002, 2004, and 2007, respectively. His research focuses on spectrum issues in radar and communication systems, and has been sponsored by the National Science Foundation and the Naval Research Laboratory. He has focused his work on the application of microwave circuit technology and measurements, combined with intelligent optimization algorithms, to creating reconfigurable transmitters. He serves as the general chair of the annual Texas Symposium on Wireless and Microwave Circuits and Systems.

Lawrence Cohen (M'87—SM'12) has been involved in electromagnetic compatibility (EMC) engineering and management, shipboard antenna integration, and radar system design for 33 years. In this capacity, he has worked in the areas of shipboard electromagnetic interference problem identification, quantification and resolution, mode-stirred chamber research, and radar absorption material design, test, and integration. In March of 2007, Mr. Cohen acted as the Navy's principal investigator in the assessment of radar emissions on a WiMAX network. Additionally, he has acted as the principal investigator for various radar programs, including the radar transmitter upgrades. Currently, he is involved with identifying and solving spectrum conflicts between radar and wireless systems, as well as research into spectrally cleaner power amplifier designs, tube, and solid state.

Mr. Cohen received a B.S. degree in electrical engineering from The George Washington University in 1975 and a M.S. degree in Electrical Engineering from Virginia Tech in 1994. He is certified as an EMC engineer by the National Association of Radio and Telecommunications Engineers. Larry served as the technical program chairman for the IEEE 2000 International Symposium on EMC and was elected for a three-year term to the IEEE EMC Society Board of Directors in 1999 and 2009. He is also a member of the IEEE EMC Society Technical Committee 6 for Spectrum Management. For the past 26 years, he has been employed by the Naval Research Laboratory in Washington, DC.



Robert J. Marks, II (S'71—M'72—SM'83—F'94) is a distinguished professor of electrical and computer engineering at Baylor University, Waco, TX. He is a Fellow of IEEE and the Optical Society of America. His most recent books are *Handbook of Fourier Analysis and Its Applications* (Oxford University Press, 2009), and *Biological Information—New Perspectives* (Singapore: World Scientific, 2013), coedited by M. J. Behe, W. A. Dembski, B. L. Gordon, and J. C. Sanford.